

Inversion of absorption spectral data for relaxation matrix determination. I. Application to line mixing in the 106←000 overtone transition of HCN

Robert Boyd, Tak-San Ho, and Herschel Rabitz
Department of Chemistry, Princeton University, Princeton, New Jersey 08544

Daniele Romanini^{a)} and Kevin Lehmann
Department of Chemistry, Princeton University, Princeton, New Jersey 08544

(Received 17 December 1996; accepted 30 September 1997)

A new method of extracting the relaxation matrix directly from absorption spectral data is formulated and applied to R-branch line mixing in HCN. The formulation makes use of a general iterative inversion algorithm based upon first-order sensitivity analysis and Tikhonov regularization. The recovered relaxation matrices describe line mixing much better than those derived from the fitting laws currently in use, and the inversion algorithm usually converges within just three iterations. This formulation presents the first known method for extracting the imaginary, off-diagonal elements of the relaxation matrix. © 1998 American Institute of Physics.
[S0021-9606(98)01802-9]

I. INTRODUCTION

The familiar description of the shape of absorption lines as the Lorentzian becomes inadequate as pressure broadening causes adjacent lines to overlap and merge in a nonlinear manner. This phenomenon, known as line mixing, can be attributed to inelastic collisions that transfer coherence among the rovibrational transitions of overlapping lines. Line mixing has practical applications in the fields of atmospheric science and combustion diagnostics and, in addition, can provide information on collision dynamics and the underlying intermolecular potential.¹ It is therefore highly desirable to formulate a good model of this phenomenon in order to accurately describe and predict such pressure-broadened spectra, as well as to probe the dynamics and the potential.

The theory of line mixing was pioneered by Anderson,² Baranger,³ and Koleb and Griem,⁴ and reformulated by Fano⁵ by adapting methods from scattering theory to the Liouville representation of density matrices. The governing quantity within this formalism is the relaxation operator $\langle M_c(\nu) \rangle$, first introduced by Zwanzig.⁶ This underlying quantity $\langle M_c(\nu) \rangle$ uniquely determines the pressure-broadened spectra and, in addition, provides a theoretical connection to the collision dynamics and the intermolecular potential.

Within the impact approximation,⁷ the frequency-dependent $\langle M_c(\nu) \rangle$ operator reduces to a frequency-independent relaxation matrix, \mathbf{W} , whose elements are directly proportional to the collision cross sections thermally averaged over collision velocity.⁸ Current parametric models for the \mathbf{W} matrix, such as the physically based energy-corrected-sudden (ECS) inelastic rate scaling law,⁹ and simple empirical models such as the modified exponential gap (MEG) law and the power-exponential gap (PEG) law,¹⁰

typically fit pressure-broadened spectra only moderately well. Hence, the development of an algorithm to extract a \mathbf{W} matrix from laboratory data that is capable of describing line mixing more precisely would be useful. To this end, an inversion method is presented to determine a suitable \mathbf{W} matrix from experimentally determined absorption spectra. The algorithm, based on the Tikhonov regularization procedure for ill-posed problems, has been successfully applied to the determination of potential surfaces using data from elastic¹¹ and inelastic¹² scattering, gas-surface scattering,¹³ and rovibrational spectroscopy.¹⁴

In this paper, the R branch of HCN is considered in detail as a case study. Recently, Romanini and Lehmann¹⁵ have reported the overtone absorption spectra for the 106←000 (1=CN, 0=bend, 6=CH) transition in HCN, measured at room temperature over a pressure range of 28.4 to 724.8 Torr. The measurements were obtained using cavity ring-down spectroscopy, resulting in a very good signal-to-noise ratio, with resolution limited only by the pulsed dye laser ($0.04 \text{ cm}^{-1} \pm 50\%$). The high quality of this data makes it ideal for purposes of inversion.

The subsequent parts of this paper are organized as follows: In Sec. II A, the relevant elements from the theory of line mixing are presented along with the necessary forward sensitivity analysis. The inversion algorithm is described in Sec. II B, and the results of an inversion using data obtained via simulation for the R branch of HCN are given in Sec. III. In Sec. IV, the inversion results using the experimental data of Romanini and Lehmann are presented and, finally, a brief summary with concluding remarks is given in Sec. V.

II. THEORY

A. Forward analysis

Within the impact approximation, the absorption coefficient $\kappa(\nu)$ describing the overlapping of spectral lines can be written as¹⁶

^{a)}Current address: Laboratoire de Spectrométrie Physique—CNRS URA 08, Université J. Fourier/Grenoble, B.P. 87—38402 Saint Martin d'Hères Cedex, France.

$$\kappa(\nu) = \frac{n}{\pi} \Im m(\mathbf{d} \cdot \mathbf{G}^{-1} \cdot \rho \cdot \mathbf{d}), \quad (1)$$

where ν is the frequency, n is the molecular density, \mathbf{d} is a vector of transition amplitudes, ρ is a diagonal matrix composed of population differences, and \mathbf{G} is a complex matrix defined as

$$\mathbf{G} = \nu \mathbf{I} - \mathbf{v}^0 - i P \mathbf{W}, \quad (2)$$

with \mathbf{I} representing the identity matrix, \mathbf{v}^0 a diagonal matrix of transition frequencies, P the pressure, and \mathbf{W} the relaxation matrix. The real, diagonal elements of the \mathbf{W} matrix are the broadening coefficients γ_I , and the imaginary, diagonal elements are the pressure shifts $\Delta \nu_I^0$. In the limit that all of the off-diagonal elements of \mathbf{W} tend toward zero, γ_I represents the width of the Lorentzian describing the line shape, and $\Delta \nu_I^0$ the shift in the position of the line from ν_{IJ}^0 . The real, off-diagonal elements are related to the collision rates Γ_{JK} by the relation $\mathbf{W}_{JK} = -F \Gamma_{JK}$, where F is an empirical factor accounting for such mechanisms as dephasing and elastic reorientation.¹⁵ All of the rate laws currently in use model only Γ_{JK} , with γ_I often obtained using the sum rule.¹ A physical description of the imaginary, off-diagonal elements is obscure, and hence no scaling law-like model is available, prompting most researchers to arbitrarily set all of the elements to zero.

The computation of $\kappa(\nu)$ is simplified considerably by defining the frequency-independent \mathbf{H} matrix,

$$\mathbf{H} = \mathbf{v}^0 + i P \mathbf{W}, \quad (3)$$

and diagonalizing it via a similarity transform to obtain the eigenvalues ω_i :

$$\mathbf{\Omega} = \mathbf{A}^{-1} \cdot \mathbf{H} \cdot \mathbf{A}, \quad (4)$$

where $\Omega_{IJ} = \delta_{IJ} \omega_I$. Since, for a given ν , \mathbf{G} differs from \mathbf{H} by a constant diagonal matrix, \mathbf{G} is also diagonalized by \mathbf{A} , and Eq. (1) can be written¹⁶ as

$$\kappa(\nu) = \frac{n}{\pi} \Im m \sum_J \left(\frac{(\mathbf{d} \cdot \mathbf{A})_J (\mathbf{A}^{-1} \cdot \rho \cdot \mathbf{d})_J}{(\nu - \omega_J)} \right). \quad (5)$$

From Eq. (1) it can be readily seen that adding a small variation to \mathbf{G} (i.e., $\delta \mathbf{G}$) results in the addition of a response $\delta \kappa(\nu)$ to $\kappa(\nu)$ according to the relation

$$\kappa(\nu) + \delta \kappa(\nu) = \frac{n}{\pi} \Im m(\mathbf{d} \cdot (\mathbf{G} + \delta \mathbf{G})^{-1} \cdot \rho \cdot \mathbf{d}). \quad (6)$$

In order to avoid the inversion of a sum of matrices, $(\mathbf{G} + \delta \mathbf{G})^{-1}$ can be expanded as

$$\begin{aligned} (\mathbf{G} + \delta \mathbf{G})^{-1} &= [\mathbf{G}(\mathbf{I} + \mathbf{G}^{-1} \delta \mathbf{G})]^{-1} \\ &= (\mathbf{I} + \mathbf{G}^{-1} \delta \mathbf{G})^{-1} \mathbf{G}^{-1} \\ &= (\mathbf{I} - \mathbf{G}^{-1} \delta \mathbf{G} + \dots) \mathbf{G}^{-1} \\ &= \mathbf{G}^{-1} - \mathbf{G}^{-1} \delta \mathbf{G} \mathbf{G}^{-1} + \dots \end{aligned} \quad (7)$$

Also, from Eq. (2), it can be seen that $\delta \mathbf{G} = -i P \delta \mathbf{W}$; hence

$$(\mathbf{G} + \delta \mathbf{G})^{-1} = \mathbf{G}^{-1} + i P \mathbf{G}^{-1} \delta \mathbf{W} \mathbf{G}^{-1} + \dots \quad (8)$$

Substituting the result of Eq. (8) into Eq. (6), keeping first-order terms only, and subtracting Eq. (1) yields the following:

$$\delta \kappa(\nu) = \frac{n P}{\pi} \Re e(\mathbf{d} \cdot \mathbf{G}^{-1} \delta \mathbf{W} \mathbf{G}^{-1} \cdot \rho \cdot \mathbf{d}). \quad (9)$$

In order to simplify the computation, the vectors \mathbf{Q} and \mathbf{R} are introduced:

$$\mathbf{Q}_J(\nu) = \sum_I \left(\frac{(\mathbf{d} \cdot \mathbf{A})_I \mathbf{A}_{IJ}^{-1}}{(\nu - \omega_I)} \right); \quad (10a)$$

$$\mathbf{R}_K(\nu) = \sum_L \left(\frac{\mathbf{A}_{KL} (\mathbf{A}^{-1} \cdot \rho \cdot \mathbf{d})_L}{(\nu - \omega_L)} \right). \quad (10b)$$

Equation (9) now become

$$\delta \kappa(\nu) = \frac{n P}{\pi} \Re e \sum_J \sum_K [\mathbf{Q}_J(\nu) \mathbf{R}_K(\nu) \delta \mathbf{W}_{JK}]. \quad (11)$$

Separating the real and imaginary parts of the following as $\delta \mathbf{W} = \delta \mathbf{W}' + i \delta \mathbf{W}''$, $\mathbf{Q}(\nu) = \mathbf{Q}'(\nu) + i \mathbf{Q}''(\nu)$, and $\mathbf{R}(\nu) = \mathbf{R}'(\nu) + i \mathbf{R}''(\nu)$, expressions can be written for the real sensitivity matrices $\mathbf{K}'(\nu)$ and $\mathbf{K}''(\nu)$, collectively denoted as \mathbf{K} :

$$\mathbf{K}'_{JK}(\nu) \equiv \frac{\partial \kappa(\nu)}{\partial \mathbf{W}'_{JK}} = \frac{n P}{\pi} [\mathbf{Q}'_J(\nu) \mathbf{R}'_K(\nu) - \mathbf{Q}''_J(\nu) \mathbf{R}''_K(\nu)]; \quad (12a)$$

$$\begin{aligned} \mathbf{K}''_{JK}(\nu) &\equiv \frac{\partial \kappa(\nu)}{\partial \mathbf{W}''_{JK}} \\ &= - \frac{n P}{\pi} [\mathbf{Q}'_J(\nu) \mathbf{R}''_K(\nu) + \mathbf{Q}''_J(\nu) \mathbf{R}'_K(\nu)]. \end{aligned} \quad (12b)$$

Equation (11) may now be expressed as

$$\delta \kappa(\nu) = \sum_J \sum_K [\mathbf{K}'_{JK}(\nu) \delta \mathbf{W}'_{JK} + \mathbf{K}''_{JK}(\nu) \delta \mathbf{W}''_{JK}]. \quad (13)$$

Direct inversion, or a least-squares fit, of the matrix equation to obtain $\delta \mathbf{W}$ is generally not possible, since empirically it is found that for all ν the $\mathbf{K}(\nu)$ matrices are ill conditioned. At any given ν , the $\mathbf{K}(\nu)$ matrices have some diagonal matrix elements that are very small, and hence classical inversion schemes such as the Gauss–Siedel iterative method must also fail. However, Eq. (13) relates infinitesimal changes in $\kappa(\nu)$ to those in \mathbf{W}_{JK} in a way that is analogous to the discretized version of a Fredholm integral equation of the general form $\delta a(x) = \sum_i \int k_i(x, y) \delta b_i(y) dy$. An iterative solution to an equation of this form has been presented in a recent paper,¹² based on the inversion algorithm of Ho and Rabitz,¹¹ which draws on the Tikhonov regularization scheme. A method of inversion based on that algorithm shall be developed in Sec. II B.

The line mixing theory presented thus far does not take into account Doppler broadening due to translational motion. Hence, it is necessary to convolve $\kappa(\nu)$ if it is to be compared with an experimentally determined spectrum.⁶

$$\kappa(\nu) \rightarrow \int D(\nu - \nu', \sigma_{\text{Dop}}) \kappa(\nu') d\nu', \quad (14a)$$

where $D(\nu - \nu', \sigma_{\text{Dop}})$ is the appropriate Doppler distribution function (Gaussian, Voigt, Rautian, etc.), and $\sigma_{\text{Dop}} = v_0(2k_B T/Mc^2)^{1/2}$, where v_0 is the band origin, is assumed to be constant over a relevant region of the spectrum. Here the parameters are the temperature T , pressure P , and mass M of the molecule. For purposes of inversion, the convolution of $\kappa(\nu)$ necessitates an identical convolution of both $\mathbf{K}(\nu)$ matrices:

$$\mathbf{K}(\nu) \rightarrow \int D(\nu - \nu', \sigma_{\text{Dop}}) \mathbf{K}(\nu') d\nu'. \quad (14b)$$

In addition, if a comparison with laboratory data is to be made, both $\kappa(\nu)$ and $\mathbf{K}(\nu)$ may have to be further convolved, e.g., with a Gaussian function of standard deviation σ_{res} , to account for the finite resolution of the measurement apparatus:

$$\kappa(\nu) \rightarrow \frac{1}{\sqrt{2\pi}\sigma_{\text{res}}} \int \kappa(\nu') \exp[-(\nu - \nu')^2/2\sigma_{\text{res}}^2] d\nu'; \quad (15a)$$

$$\mathbf{K}(\nu) \rightarrow \frac{1}{\sqrt{2\pi}\sigma_{\text{res}}} \int \mathbf{K}(\nu') \exp[-(\nu - \nu')^2/2\sigma_{\text{res}}^2] d\nu'. \quad (15b)$$

B. Method of inversion

The objective of the inversion algorithm presented here is to obtain a relaxation matrix \mathbf{W} , which, when used to theoretically calculate a given absorption spectrum, reproduces to within experimental error the spectrum $\kappa(\nu)$ obtained from good laboratory sources. It is implicitly assumed that the transition frequencies \mathbf{v}^0 , transition amplitudes \mathbf{d} , and population differences ρ can be obtained via a separate method. The first step in the inversion scheme is to choose a reference relaxation matrix \mathbf{W}^0 , such as can be obtained from one of the fitting laws. Next, Eqs. (5) and (12) are

solved to obtain an approximate spectrum $\kappa^0(\nu)$ and its corresponding sensitivities $\mathbf{K}(\nu)$, which are then convolved according to Eqs. (14) and (15). It should be noted that, in practice, all measurements of $\kappa(\nu)$ will be discrete $\kappa(\nu_q)$, measured at N frequencies from ν_1 to ν_N , and that must be compared with discrete $\kappa^0(\nu_q)$, calculated at identical frequencies. Since the magnitudes of $\kappa(\nu_q)$, often expressed in arbitrary units, and $\kappa^0(\nu_q)$ will, in general, be different, it is necessary to multiply $\kappa^0(\nu_q)$ and the discrete $\mathbf{K}(\nu_q)$ by an appropriate normalization factor Z :

$$Z = \frac{\sum_{p=1}^N \kappa(\nu_p)}{\sum_{p=1}^N \kappa^0(\nu_p)}. \quad (16)$$

According to the Tikhonov regularization procedure, an approximate solution to Eq. (13) can be obtained by minimizing the following functional $\Phi(\alpha, \delta\mathbf{W})$:

$$\Phi(\alpha, \delta\mathbf{W}) \equiv \left\| \left(\sum_J \sum_K \mathbf{K}'_{JK}(\nu_q) \delta\mathbf{W}'_{JK} + \mathbf{K}''_{JK}(\nu_q) \delta\mathbf{W}''_{JK} \right) - \delta\kappa(\nu_q) \right\|^2 + \alpha \left(\sum_J \sum_K \|\delta\mathbf{W}'_{JK}\|^2 + \|\delta\mathbf{W}''_{JK}\|^2 \right), \quad (17)$$

where zeroth-order regularization has been chosen, $\delta\kappa(\nu_q) = \kappa(\nu_q) - \kappa^0(\nu_q)$, and the norms for $\delta\mathbf{W}'$ and $\delta\mathbf{W}''$ are understood in the Frobenius sense as a sum over the square of each element. The regularization parameter α may be optimally determined by minimizing the differences between $\kappa(\nu_q)$ and a trial spectrum $\kappa^{\text{trial}}(\nu_q)$ calculated with $\mathbf{W}^0 + \delta\mathbf{W}^{\text{trial}}(\alpha)$, i.e., by minimizing a functional $J(\alpha)$, noting that $\delta\mathbf{W}^{\text{trial}}(\alpha)|_{J(\alpha)=\min} = \delta\mathbf{W}$. The form of $J(\alpha)$ may be selected in such a manner that experimental errors $\epsilon[\kappa(\nu_q)]$ can be accounted for and random noise filtered out, e.g., by convolution with a Gaussian function of standard deviation σ_{filt} :

$$J(\alpha) = \frac{1}{N} \sum_{p=1}^N \left(\frac{(\nu_N - \nu_1) \sum_{q=1}^N [\kappa(\nu_q) - \kappa^{\text{trial}}(\nu_q)] \exp[-(\nu_p - \nu_q)^2/2\sigma_{\text{filt}}^2]}{N\sqrt{2\pi}\sigma_{\text{filt}}} \right)^2 \epsilon[\kappa(\nu_p)]. \quad (18)$$

The solution of Eq. (17) in the least squares sense is given by

$$\delta\mathbf{W}_{JK} = \sum_{p=1}^N \frac{(\delta\kappa|u_p)}{\lambda_p^2 + \alpha} \left(\sum_{q=1}^N u_p(\nu_q) \mathbf{K}_{JK}(\nu_q) \right), \quad (19)$$

where the inner product $(\delta\kappa|u_p)$ is given by

$$(\delta\kappa|u_p) = \sum_{q=1}^N \delta\kappa(\nu_q) u_p(\nu_q), \quad (20)$$

and λ_p^2 and u_p are the singular values and vectors, respectively, of the relevant Gram matrix \mathbf{M} , defined as

$$\mathbf{M}_{mn} \equiv \sum_J \sum_K [\mathbf{K}'_{JK}(\nu_m) \mathbf{K}'_{JK}(\nu_n) + \mathbf{K}''_{JK}(\nu_m) \mathbf{K}''_{JK}(\nu_n)]. \quad (21)$$

Once $\delta\mathbf{W}$ has been calculated, it is added to \mathbf{W}^0 to obtain a new, improved relaxation matrix. The sum is then used

as the new reference relaxation matrix for the next iteration. Convergence is achieved when $\kappa^0(\nu_q)$ agrees with $\kappa(\nu_q)$ to within experimental error.

III. A TEST OF THE INVERSION ALGORITHM

In order to test the algorithm described in the preceding section, it was thought prudent to first apply it to synthetic data where the \mathbf{W} matrix is “known,” rather than proceed directly to experimental data, where such factors as noise and the finite instrumental resolution, often imprecisely known, might obscure any deficiencies of the method. Only after testing and refinement, if necessary, may it be applied with some level of confidence to experimental data. Using a variation of the random-phase approximation,¹ Romanini and Lehmann determined that the MEG scaling law gave the best overall fit to their HCN R-branch data,¹⁵ with many of the relevant parameters being obtained from a previous Q-branch study of HCN,⁸ where, e.g., the calculation of certain parameters is less problematic than in the R branch.¹⁷ All imaginary elements of the \mathbf{W} matrix, including the diagonal elements, were arbitrarily set to zero.¹⁵ Synthetic data generated from the MEG-law \mathbf{W} matrix for (1) a low-pressure case of 28.4 Torr and (2) an intermediate-pressure case of 379.9 Torr, were chosen to test the algorithm. Doppler broadening and related effects were simulated via a Rautian distribution function [see Eq. (14)], and an instrument function of $\sigma_{\text{res}}=0.04 \text{ cm}^{-1}$ was factored in [see Eq. (15)]. An inversion seeking the recovery of both the real and imaginary elements of \mathbf{W} was also run at $P=28.4$ Torr and an initial guess $\mathbf{W}^0=0.5*\mathbf{W}^{\text{MEG}}$ to see how faithfully $\mathbf{W}''=0$ was recovered. Some relatively small nonzero elements did arise in the recovered elements of \mathbf{W}'' that oscillated around zero. The results confirm the stability of the algorithm, and following Romanini and Lehmann, all imaginary elements of \mathbf{W} were arbitrarily set to zero, and only the real part of the \mathbf{W} matrix was sought to be recovered in the inversions described below.

It should be noted that σ_{filt} in Eq. (18) was chosen such that it would be suitable for the HCN R-branch experimental data. Since there seemed to be relatively more noise far away from the band head, and in order to preserve all the features close to the band head (i.e., toward ν_N), σ_{filt} was chosen to be

$$\sigma_{\text{filt}}(\nu_q) = \frac{0.555 \text{ cm}^{-1}}{\nu_1 - \nu_N + 0.1 \text{ cm}^{-1}} (\nu_q - \nu_N - 0.1 \text{ cm}^{-1}). \quad (22)$$

This function smoothed out the noise well, yet retained the bulk of the features of the spectrum. This form for σ_{filt} was used for all inversions reported in this work.

Sensitivities with respect to the diagonal \mathbf{W} matrix elements are shown in Fig. 1 for a pressure of 28.4 Torr, and an additional sensitivity calculation, not displayed for brevity, was run for 379.9 Torr; both are pressures for which experimental data are available. At both pressures, the magnitudes of $\mathbf{K}'_{JJ}(\nu)$ and $\mathbf{K}''_{JJ}(\nu)$ are comparable with each other, indicating the nearly equal importance of the broadening coeffi-

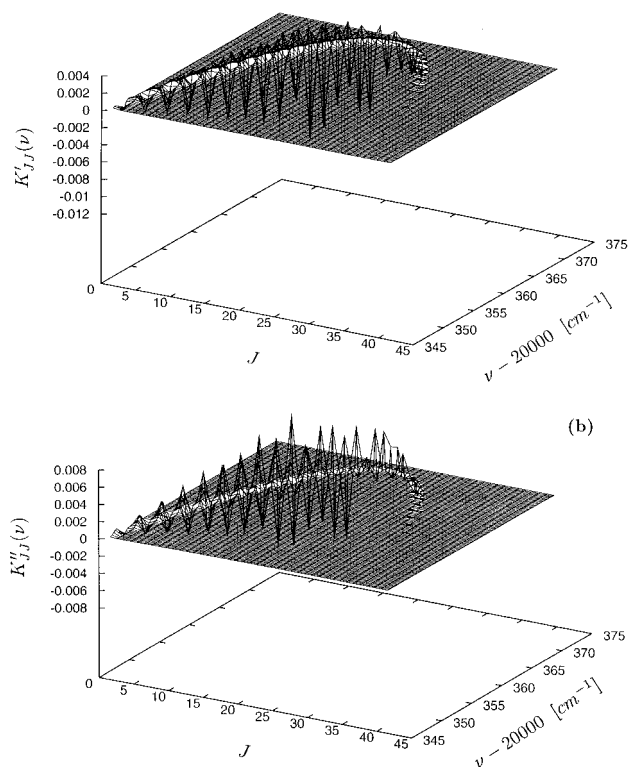


FIG. 1. Sensitivities with respect to $\mathbf{W}_{JJ}^{\text{MEG}}$ at 28.4 Torr, measured in arbitrary (though consistent) units: (a) $\mathbf{K}'_{JJ}(\nu)$ and (b) $\mathbf{K}''_{JJ}(\nu)$.

cients and the pressure shifts in determining the spectrum. Although the trends are quite similar at either pressure, the magnitude of the sensitivities is much larger for $P=379.9$ Torr, and the sensitivities possess a somewhat richer structure at the higher pressure. This is consistent with the fact that pressure-broadening effects increase with increasing pressure. However, for purposes of inversion, this increased sensitivity with increasing pressure is offset somewhat by the simultaneous diminishing of spectral features. For both $\mathbf{K}'_{JJ}(\nu)$ and $\mathbf{K}''_{JJ}(\nu)$, a characteristic arclike feature appears in the plots for either pressure, indicating that any given area of the spectrum is sensitive to only a very small number of \mathbf{W}_{JJ} values. This is quite reasonable, since one would expect those regions of the spectrum immediately surrounding any given line to be most sensitive to its respective phase-shift and pressure-broadening coefficients, as well as those immediately surrounding them in J , yet relatively insensitive to phase shifts and pressure-broadening far removed in J . The arclike structure also falls off in magnitude beginning around $J=30$, which is consistent with the $J=40$ cutoff in Eq. (5) used by Romanini and Lehmann in their theoretical computations.¹⁵ Plots of $\mathbf{K}'_{JK}(\nu)$ and $\mathbf{K}''_{JK}(\nu)$ for $J \neq K$, not shown for brevity, also typically display arclike structures, and possess elements of significant magnitude only for $J=K \pm 1, 2, \text{ or } 3$. For sensitivities with respect to the real, off-diagonal \mathbf{W} matrix elements, this limited range of significant $\mathbf{K}'_{JK}(\nu)$ elements is consistent with use of the MEG law.

At the lower pressure, it was determined that reasonable inversion results could be obtained if the initial guess \mathbf{W}^0 was within $\pm 50\%$ of the model \mathbf{W}^{MEG} . The results for \mathbf{W}^0

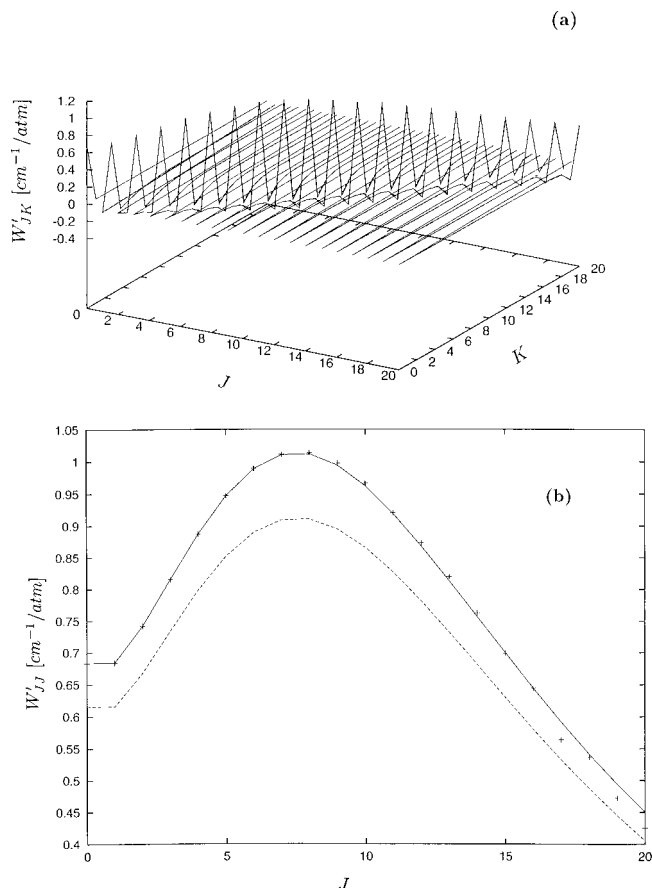


FIG. 2. The real part of the \mathbf{W} matrix showing the inversion results from data obtained via simulation for 28.4 Torr and $\mathbf{W}^0 = 0.9 * \mathbf{W}^{\text{MEG}}$: (a) \mathbf{W}^{MEG} (solid) and \mathbf{W}^{rec} (dashed); (b) $\mathbf{W}_{JJ}^{\text{MEG}}$ (solid), \mathbf{W}_{JJ}^0 (dashed), and $\mathbf{W}_{JJ}^{\text{rec}}$ (+). All \mathbf{W} matrix elements are in $\text{cm}^{-1}/\text{atm}$.

$= 0.9 * \mathbf{W}^{\text{MEG}}$, a moderately good guess, are shown in Figs. 2 and 3. The recovered matrix \mathbf{W}^{rec} is in good overall agreement with \mathbf{W}^{MEG} [Fig. 2(a)], and, in particular, $\mathbf{W}_{JJ}^{\text{rec}}$ is in excellent agreement with the model for $J \leq 16$ [see Fig. 2(b)].

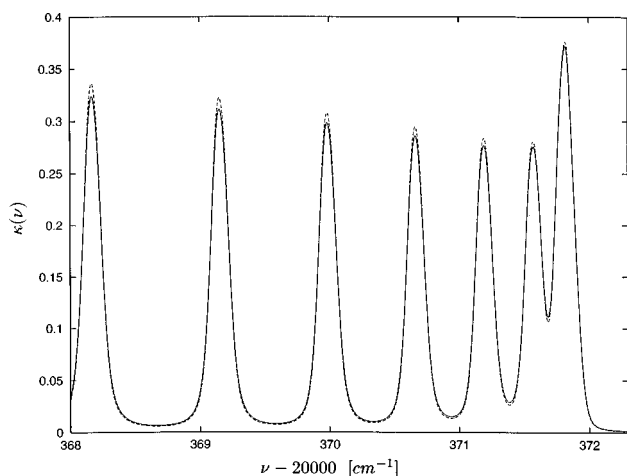


FIG. 3. The recovered and measured spectrum from the inversions using data obtained via simulation for 28.4 Torr and $\mathbf{W}^0 = 0.9 * \mathbf{W}^{\text{MEG}}$: $\kappa^{\text{MEG}}(\nu)$ (solid), $\kappa^0(\nu)$ (heavy dashed), and $\kappa^{\text{rec}}(\nu)$ (light dashed; coincides with the solid line). All $\kappa(\nu)$ are measured in arbitrary units.

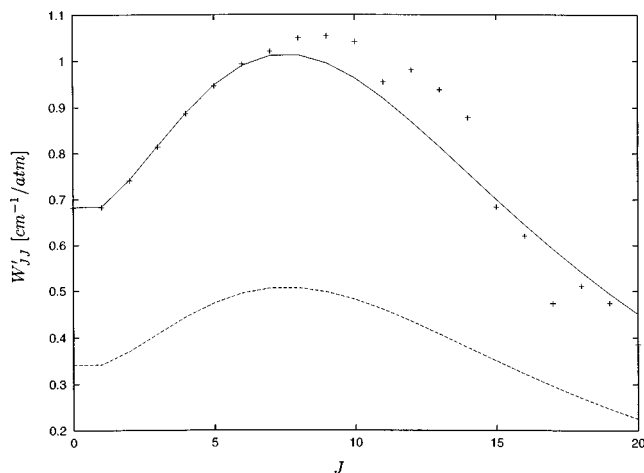


FIG. 4. Diagonal elements of the real \mathbf{W} matrix showing the inversion results from data obtained via simulation for 28.4 Torr and $\mathbf{W}^0 = 0.5 * \mathbf{W}^{\text{MEG}}$: $\mathbf{W}_{JJ}^{\text{MEG}}$ (solid), \mathbf{W}_{JJ}^0 (dashed), and $\mathbf{W}_{JJ}^{\text{rec}}$ (+). All \mathbf{W} matrix elements are in $\text{cm}^{-1}/\text{atm}$.

The lower values of J are most important for line mixing, especially at low pressures. As shown in Fig. 3, the spectrum $\kappa^{\text{rec}}(\nu)$ calculated from \mathbf{W}^{rec} is in superb agreement with the model spectrum $\kappa^{\text{MEG}}(\nu)$, even at the band head, and convergence was achieved within three iterations. (The full range of the spectrum is not shown here for brevity; it added nothing new to what is already shown in Fig. 3.)

The results for $\mathbf{W}^0 = 0.5 * \mathbf{W}^{\text{MEG}}$, a quite poor estimate of the line mixing, are given in Figs. 4 and 5; the full \mathbf{W} -matrix plots were omitted for brevity. Although the inversion results are not quite as good as for the previous case, nevertheless, very reasonable agreement between the most sensitive elements of the recovered and model \mathbf{W} matrices is still obtained, with excellent agreement between $\mathbf{W}_{JJ}^{\text{rec}}$ and $\mathbf{W}_{JJ}^{\text{MEG}}$ for $J \leq 7$ (see Fig. 4). Even though the diagonal elements for $J > 7$ did not match the model well, there was still some overall improvement from the initial guess. Here $\kappa^{\text{rec}}(\nu)$ agrees

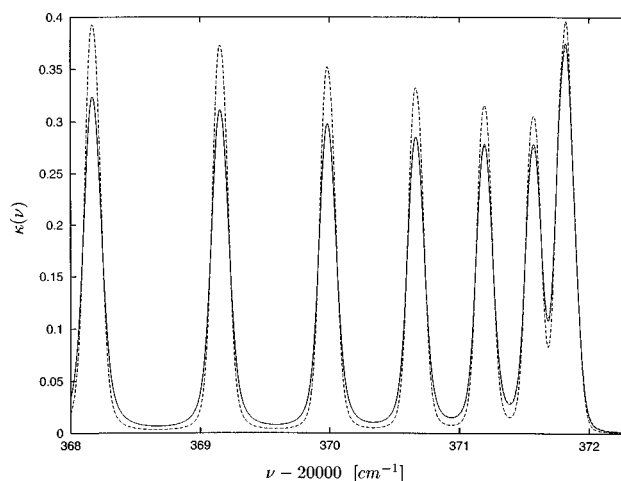


FIG. 5. The recovered and measured spectrum from the inversions using data obtained via simulation for 28.4 Torr and $\mathbf{W}^0 = 0.5 * \mathbf{W}^{\text{MEG}}$: $\kappa^{\text{MEG}}(\nu)$ (solid), $\kappa^0(\nu)$ (heavy dashed), and $\kappa^{\text{rec}}(\nu)$ (light dashed). All $\kappa(\nu)$ are measured in arbitrary units.

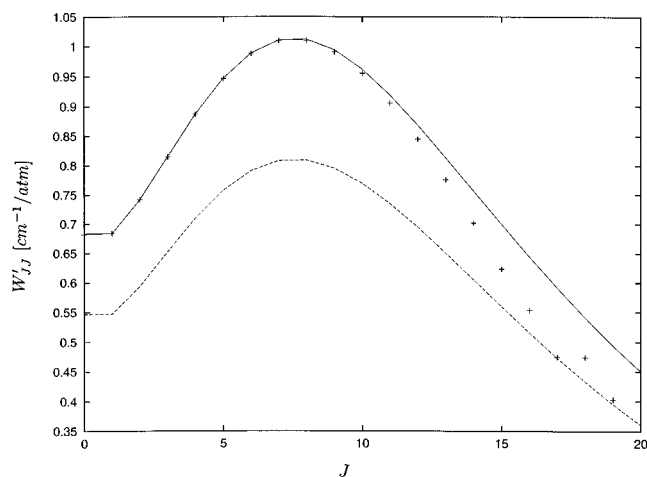


FIG. 6. Diagonal elements of the real \mathbf{W} matrix showing the inversion results from data obtained via simulation for 379.9 Torr and $\mathbf{W}^0 = 0.8 * \mathbf{W}^{\text{MEG}}$. See Fig. 4 for fonts. All \mathbf{W} matrix elements are in $\text{cm}^{-1}/\text{atm}$.

well with $\kappa^{\text{MEG}}(\nu)$, especially considering how poorly the initial guess predicts the spectrum, with some minor discrepancy at the band head lingering (see Fig. 5). Convergence was again achieved within three iterations.

At the higher pressure, it was found that good inversion results could be achieved if \mathbf{W}^0 was within $\pm 20\%$ of the model. The inversion results for $\mathbf{W}^0 = 0.8 * \mathbf{W}^{\text{MEG}}$ are presented in Figs. 6 and 7, and, once again, show quite good overall agreement between \mathbf{W}^{rec} and \mathbf{W}^{MEG} . The diagonal elements are recovered well for $J < 10$ and show some improvement for $10 \leq J < 16$, but no significant improvement for $J \geq 16$, suggesting a somewhat smaller effective region of significance than predicted by the sensitivity analysis alone. This can be understood by considering the fact that, at higher pressures, the diminishing features of the spectrum, in general, reduce the overall information content of the data and heighten the nonuniqueness of the inversion problem. This improvement toward the correct \mathbf{W} matrix is reassuring. Very good overall agreement between $\kappa^{\text{rec}}(\nu)$ and $\kappa^{\text{MEG}}(\nu)$ is achieved, with some small discrepancies toward the band head (see Fig. 7). The inversion algorithm converged within five iterations. It should be noted that the general insensitivity of a spectrum predicted by the MEG law to off-diagonal elements was demonstrated by the fact that, apart from $\mathbf{W}'_{J,J\pm 1}$, very few elements recovered for any of the inversions reported above rigorously obeyed the detailed balance law, $\mathbf{W}'_{JK} = (\rho_K / \rho_J) \mathbf{W}'_{KJ}$.

IV. APPLICATION TO EXPERIMENTAL DATA

Although the structure of the absorption spectrum is richer at lower pressures, two factors make the use of very low-pressure data unattractive. The accuracy of the recovered \mathbf{W} matrix is inherently limited by the validity of the Doppler spectral distribution model used in Eq. (14) as well as by how well the resolution of the measurements is known [i.e., the instrument function in Eq. (15)]. For the former consideration, collisional (Dicke) narrowing of the (Gauss-

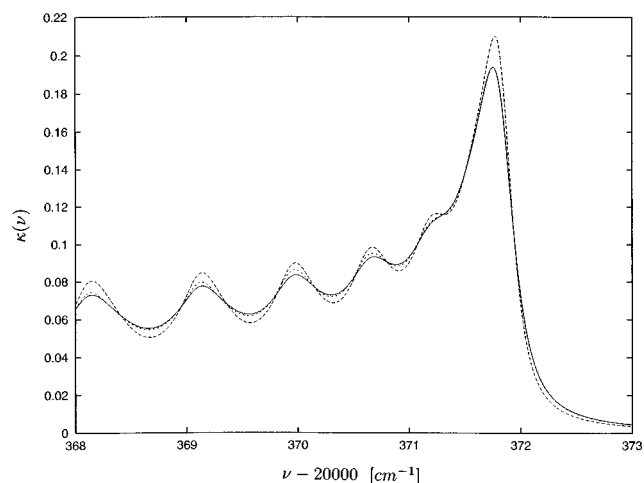


FIG. 7. The recovered and measured spectrum from the inversions using data obtained via simulation for 379.9 Torr and $\mathbf{W}^0 = 0.8 * \mathbf{W}^{\text{MEG}}$. See Fig. 5 for fonts. All $\kappa(\nu)$ are measured in arbitrary units.

ian) Doppler distribution is often modeled by a Voigt, uncorrelated Rautian (hard collision), as was chosen for this work, or Galatry (soft collision) profile, all of which neglect asymmetries. It is possible to account for asymmetries by modifying the Rautian or Galatry profiles to account for partial correlations between velocity- and state-changing collisions.¹⁸ However, at this point, it seems unclear as to which model works best when, and, indeed, if all mechanisms for broadening not accounted for in the line-shape formalism of Eqs. (1)–(13) have been exhausted.¹⁸ For the latter situation, while it is generally accepted that the frequency spread of the dye laser used to scan the spectrum is more or less Gaussian, the width of that Gaussian may not be precisely known, and may even possess a slight frequency dependence. The estimation of σ_{res} is $0.04 \text{ cm}^{-1} \pm 50\%$ for the HCN R-branch data used here. Both of these factors become less significant with increasing pressure, and by $P = 200$ Torr, for example, the imprecision in the knowledge of the instrumental resolution is effectively irrelevant. However, the diminishing of distinctive spectral features with increasing pressure, decreasing the information content of the data, means a compromise must be sought for purposes of inversion. Fortunately, even the spectrum measured at the highest pressure reported by Romanini and Lehmann ($P = 724.8$ Torr) still contains a good deal of structure. Although inversions were performed at several pressures between $P = 200$ and $P = 724.8$ Torr for which experimental data are available, only the results for $P = 379.9$ and $P = 724.8$ Torr are reported below for the sake of brevity. These two inversions typify what was found at the other pressures.

The inversion results for $P = 379.9$ Torr, starting with $\mathbf{W}'^0 = \mathbf{W}^{\text{MEG}}$, $\mathbf{W}''^0 = 0$, are presented in Figs. 8–10. The recovered spectrum $\kappa^{\text{rec}}(\nu)$ is in excellent agreement with the experimental spectrum $\kappa^{\text{exp}}(\nu)$ [see Fig. 8(a)], fitting the spectrum well within experimental error. For comparison, the MEG law prediction is shown in Fig. 8(b). The spectrum at this pressure represents the best prediction given by \mathbf{W}^{MEG}

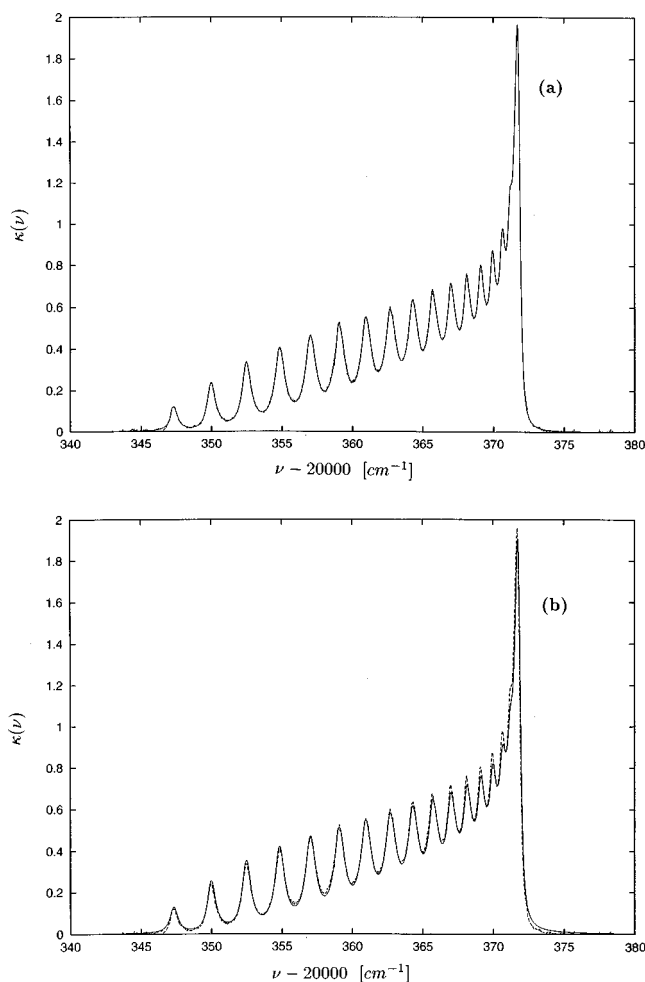


FIG. 8. The recovered and measured spectrum from the inversions using experimental data measured at 379.9 Torr: (a) $\kappa^{\text{rec}}(\nu)$ (solid) and $\kappa^{\text{exp}}(\nu)$ (dashed); (b) $\kappa^{\text{MEG}}(\nu)$ (solid) and $\kappa^{\text{exp}}(\nu)$ (dashed). All $\kappa(\nu)$ measured are in arbitrary units.

for the HCN R branch.¹⁵ While fitting $\kappa^{\text{exp}}(\nu)$ moderately well, $\kappa^{\text{MEG}}(\nu)$ is particularly inadequate close to the band head. The relative size and shapes of the peaks are described much better by $\kappa^{\text{rec}}(\nu)$. Here \mathbf{W}'^{rec} possesses off-diagonal elements typically of somewhat greater magnitude than \mathbf{W}'^{MEG} [see Fig. 9(a)]. Although the recovered real, diagonal elements are in general agreement with the MEG law for $J > 10$, $\mathbf{W}'_{JJ}^{\text{rec}}$ are somewhat larger than $\mathbf{W}'_{JJ}^{\text{MEG}}$ for $J \leq 10$. The inversion results for the imaginary part of the \mathbf{W} matrix are given in Fig. 10. Although generally small in magnitude, they are interesting in that they represent the first known determination of the off-diagonal imaginary elements.¹⁹ The inversion algorithm converged within three iterations.

Inversion results for $P=724.8$ Torr are presented in Figs. 11–13. At this pressure, results for two initial guesses, (1) $\mathbf{W}'^0 = \mathbf{W}'^{\text{MEG}}$; $\mathbf{W}''^0 = 0$, and (2) $\mathbf{W}'^0 = \mathbf{W}'^{\text{rec}}$ from the previous inversion at $P=379.9$ Torr, which shall henceforth be referred to as \mathbf{W}^{380} , are given. Both inversions yielded very consistent results, and both $\kappa^{\text{rec}}(\nu)$ agree well with each other and with $\kappa^{\text{exp}}(\nu)$, fitting the data well within experimental error [see Fig. 11(a)]. The spectra predicted from

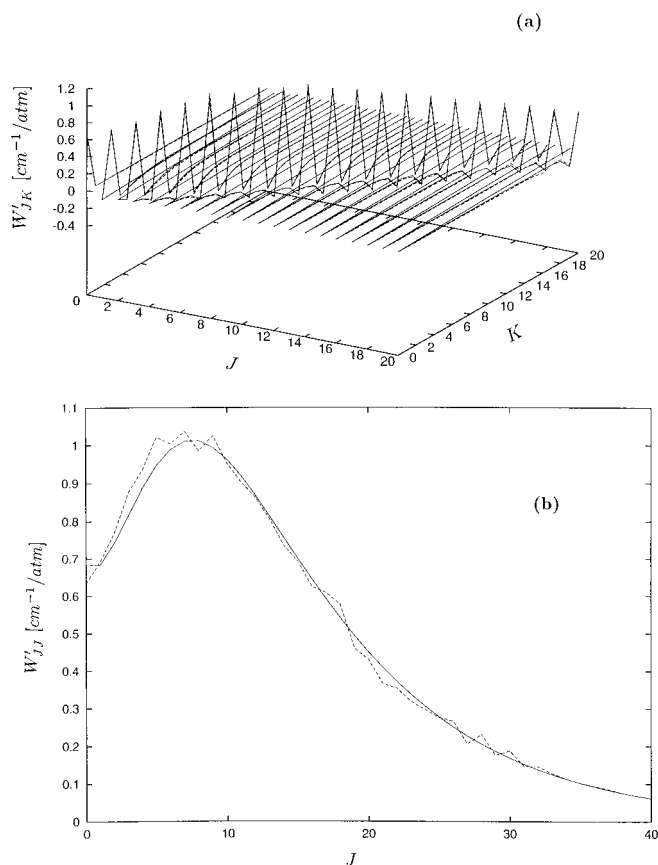


FIG. 9. The real part of the \mathbf{W} matrix showing the inversion results using experimental data measured at 379.9 Torr: \mathbf{W}'^{MEG} (solid) and \mathbf{W}'^{rec} (dashed); (a) full matrix and (b) diagonal elements. All \mathbf{W} matrix elements are in $\text{cm}^{-1}/\text{atm}$.

\mathbf{W}'^{MEG} and \mathbf{W}^{380} are shown in Figs. 11(b) and 11(c), respectively, along with $\kappa^{\text{exp}}(\nu)$. Both models predict $\kappa^{\text{exp}}(\nu)$ only moderately well, although \mathbf{W}^{380} does seem to describe the shapes of the peaks in the troublesome band head region somewhat better than \mathbf{W}'^{MEG} . However, ideally, \mathbf{W}^{380} should have predicted the spectrum at this higher pressure much better than it did. Reasons for this failure to predict $\kappa(\nu)$ better include (1) the fact that only some of the elements of \mathbf{W} are recovered to any degree of precision at a given pressure; that is, only the elements to which the data are significantly sensitive are improved upon over the initial guess. Other elements may not show any significant improvement, or may even diverge from their “true” value due to low sensitivity upon the data. At a different pressure, these elements may play a significant role in determining the spectrum. From the sensitivity analysis, these remarks seem to be especially true for the off-diagonal elements. (2) Possible inaccuracies in P, T, \mathbf{d} or possibly even ρ , for which the \mathbf{W}'^{rec} matrix would attempt to compensate in order to better fit the data. When the pressure is changed, such a \mathbf{W} matrix would not be expected to predict the spectrum well. (3) Of the same nature as (2), any discrepancy in the transition frequencies ν^0 would be compensated for and added to the pressure shifts contained in \mathbf{W}''_{JJ} [from Eq. (2), $\delta\mathbf{G} = -\delta\nu^0 - iP \delta\mathbf{W}$; the condition $\delta\nu^0 \equiv 0$ must be satisfied in order for Eqs. (8)–(13)

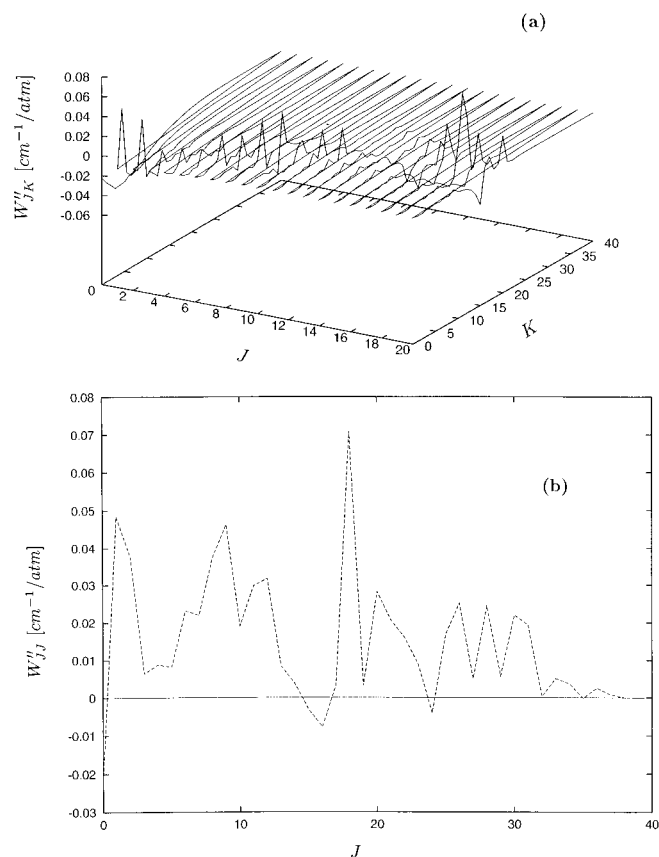


FIG. 10. The imaginary part of the \mathbf{W} matrix showing the inversion results using experimental data measured at 379.9 Torr: (a) $\mathbf{W}''^{\text{rec}}$; (b) $\mathbf{W}''_{JJ} = 0$ (solid) and $\mathbf{W}''_{JJ}^{\text{rec}}$ (dashed). All \mathbf{W} matrix elements are in $\text{cm}^{-1}/\text{atm}$.

to be strictly valid], resulting in an erroneous pressure-dependent component of the recovered \mathbf{W}''_{JJ} . Or (4), a possible overfitting of the data so that the recovered \mathbf{W} matrix reproduces the noise plus the spectrum instead of simply describing the underlying spectral pattern, resulting in a poor extrapolation to other pressures.

As with the inversion reported above, \mathbf{W}'^{rec} , starting from $\mathbf{W}^0 = \mathbf{W}^{\text{MEG}}$, possesses larger off-diagonal elements than \mathbf{W}'^{MEG} . Only very small differences exist between \mathbf{W}'^{rec} , starting from $\mathbf{W}'^0 = \mathbf{W}'^{380}$, and \mathbf{W}'^{380} itself [see Fig. 12(a)]. These slight corrections apparently yield the significant improvements seen in κ^{rec} (Fig. 11), and tend to support reason (1), above, as to why \mathbf{W}^{380} does not better predict the spectrum at $P = 724.8$ Torr. The real, diagonal elements $\mathbf{W}'_{JJ}{}^{\text{rec}}$ agree well with each other for either choice of \mathbf{W}^0 , and show, as for $P = 379.9$ Torr, somewhat larger values for $J < 10$ (however, with a few larger than the corresponding elements of $\mathbf{W}'_{JJ}{}^{380}$), as well as slightly smaller elements for $J > 10$ [Fig. 12(b)]. The recovered imaginary elements, shown in Fig. 13, while again small in magnitude, agree well with each other in shape, if not exactly in magnitude. This fact is quite reassuring, in that it seems that physically relevant elements are being recovered, considering one was recovered starting with $\mathbf{W}''^0 = 0$ and the other with $\mathbf{W}''^0 = \mathbf{W}''^{380}$. It should be noted that \mathbf{W}''^{380} possesses a somewhat different shape than $\mathbf{W}''^{\text{rec}}$; possible reasons for this

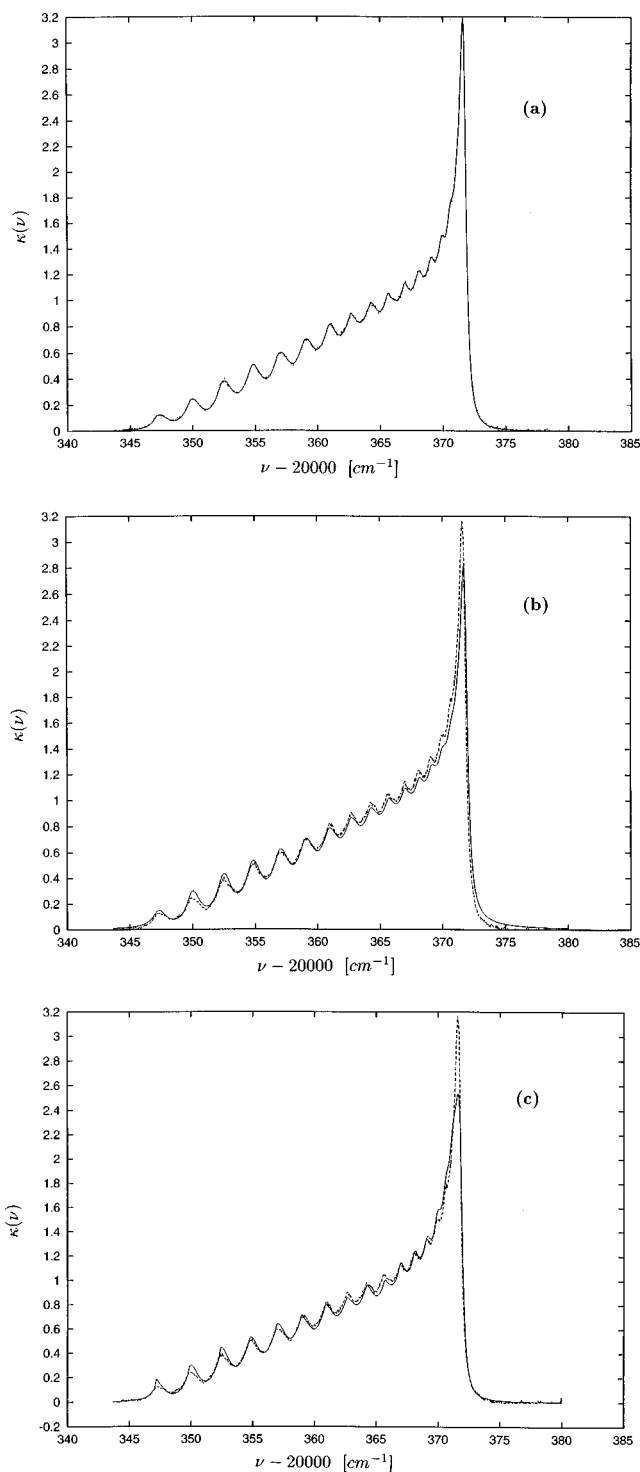


FIG. 11. The recovered and measured spectrum from the inversions using experimental data measured at 724.8 Torr: (a) $\kappa^{\text{rec}}(\nu)$ from $\mathbf{W}^0 = \mathbf{W}^{\text{MEG}}$ (solid), $\kappa^{\text{rec}}(\nu)$ from $\mathbf{W}^0 = \mathbf{W}^{380}$ (heavy dashed), and $\kappa^{\text{exp}}(\nu)$ (light dashed); (b) $\kappa^{\text{MEG}}(\nu)$ (solid) and $\kappa^{\text{exp}}(\nu)$ (dashed); (c) $\kappa^{380}(\nu)$ (solid) and $\kappa^{\text{exp}}(\nu)$ (dashed). All $\kappa(\nu)$ are measured in arbitrary units.

discrepancy were given in reason (3), above. For either choice of \mathbf{W}^0 , the algorithm converged within three iterations.

For the inversions reported above, the fact that only a few of the off-diagonal elements of \mathbf{W} are recovered to high

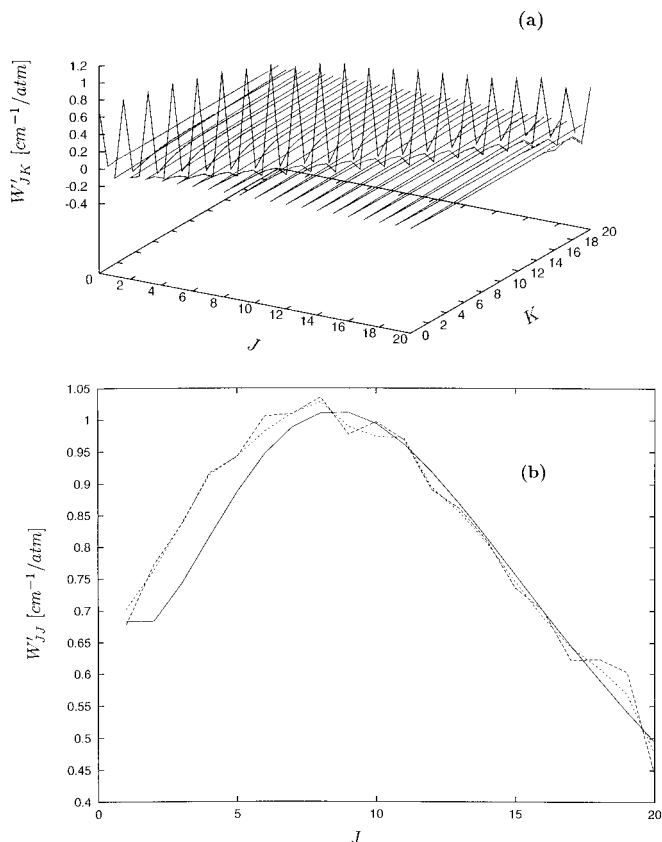


FIG. 12. The real part of the \mathbf{W} matrix showing the inversion results using experimental data measured at 724.8 Torr: (a) \mathbf{W}'^{380} (solid) and \mathbf{W}'^{rec} (dashed); (b) $\mathbf{W}'_{JJ}^{\text{MEG}}$ (solid), $\mathbf{W}'_{JJ}^{\text{rec}}$ from $\mathbf{W}^0 = \mathbf{W}^{\text{MEG}}$ (light dashed), and $\mathbf{W}'_{JJ}^{\text{rec}}$ from $\mathbf{W}^0 = \mathbf{W}^{380}$ (heavy dashed).

precision was demonstrated by the fact that many $\mathbf{W}'_{J,J\pm 1}^{\text{rec}}$ obeyed detailed balance within 1% or better, a few for $\mathbf{W}'_{J,J\pm 2}^{\text{rec}}$, and fewer still for $\mathbf{W}'_{J,J\pm 3}^{\text{rec}}$. The specific recovered elements for which a detailed balance held were different at different pressures. Although this test provides an indicator as to which elements of $\mathbf{W}'_{J,K\neq J}$ are recovered to high precision, a reformulation of the algorithm to explicitly require the recovered \mathbf{W} matrices to satisfy a detailed balance may improve the overall results. This was not reported here for brevity, since it was deemed useful to first test the algorithm without imposing a detailed balance to see how well the recovered, off-diagonal elements of \mathbf{W}' naturally obeyed the law. It shall be reported in a subsequent paper.

V. CONCLUSIONS

In this paper it has been shown that, at a given temperature and pressure, absorption spectral data can be used to recover with precision those \mathbf{W} matrix elements to which the data are sensitive. This method represents the first known technique to determine the imaginary, off-diagonal elements of the \mathbf{W} matrix.¹⁹ In the case study performed here, \mathbf{W} matrices for the 106←000 overtone transition of HCN were obtained that described the observed spectra significantly better than those based upon the population transfer rate laws, such as ECS or MEG. The somewhat limited success

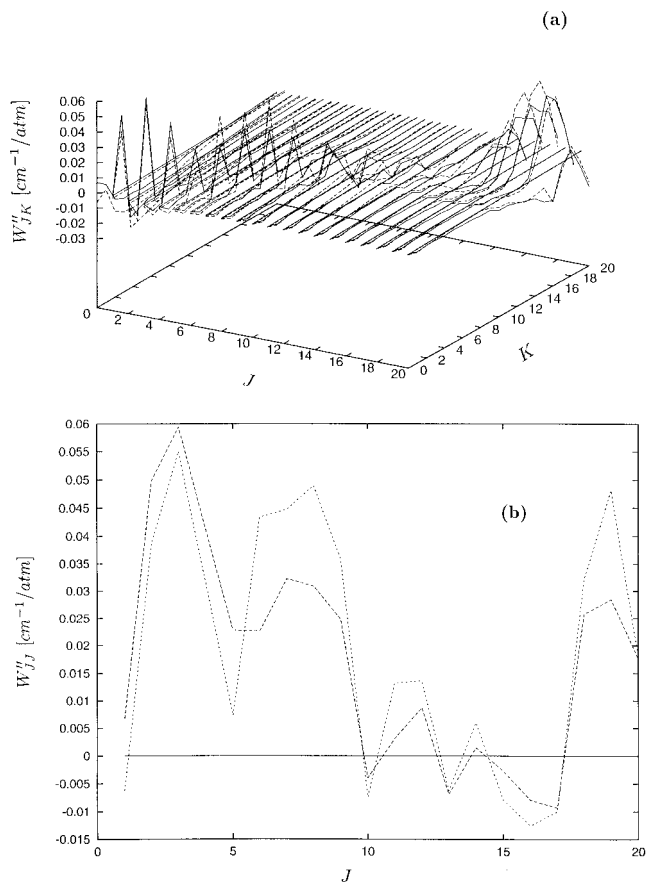


FIG. 13. The imaginary part of the \mathbf{W} matrix showing the inversion results using experimental data measured at 724.8 Torr: (a) $\mathbf{W}''^{\text{rec}}$ from $\mathbf{W}''^0 = \mathbf{W}''^{380}$ (solid) and $\mathbf{W}''_{JJ}^{\text{rec}}$ from $\mathbf{W}''^0 = 0$ (dashed); (b) $\mathbf{W}''_{JJ}^0 = 0$ (solid), $\mathbf{W}''_{JJ}^{\text{rec}}$ from $\mathbf{W}''^0 = 0$ (light dashed), and $\mathbf{W}''_{JJ}^{\text{rec}}$ from $\mathbf{W}''^0 = \mathbf{W}''^{380}$ (heavy dashed).

of the recovered \mathbf{W} matrices at the extrapolation to other pressures can be accounted for, at least in part, in that, at different pressures, the spectrum is sensitive to different elements of the \mathbf{W} matrix to which it was not at the previous pressure (and hence these elements were not recovered to any degree of precision). The inversion algorithm, based upon the Tikhonov regularization scheme, usually converges quickly, within three to five iterations.

The calculation of more accurate \mathbf{W} matrix elements gives rise to the possibilities of (1) additional inversion to obtain cross sections and even possibly the underlying intermolecular potential given data of sufficient quality; and (2) investigating the empirical F factor for off-diagonal elements, whose rigorous theoretical origin is somewhat ambiguous at this time.¹⁵ Further applications of the algorithm to different systems seems in order.

ACKNOWLEDGMENTS

The authors wish to thank A. Pine for providing his \mathbf{W} matrix software. This research was supported by the Department of Energy.

¹ See, for example, S. Green, in *Status and Future Developments in Transport Properties*, edited by W. A. Wekeham *et al.* (Kluwer Academic Pub-

- lishers, Netherlands, 1992), p. 257, and references therein.
- ²P. W. Anderson, *Phys. Rev.* **76**, 647 (1949); **86**, 809 (1952).
- ³M. Baranger, *Phys. Rev.* **111**, 481, 494 (1958); **112**, 855 (1958).
- ⁴A. C. Kolb and H. Griem, *Phys. Rev.* **111**, 514 (1958).
- ⁵U. Fano, *Phys. Rev.* **131**, 259 (1963).
- ⁶R. Zwanzig, *J. Chem. Phys.* **33**, 1338 (1960); *Phys. Rev.* **124**, 983 (1961).
- ⁷See, for example, A. Ben-Reuven, *Adv. Chem. Phys.* **33**, 235 (1975).
- ⁸A. S. Pine and J. P. Looney, *J. Chem. Phys.* **96**, 1704 (1992), and references therein.
- ⁹A. DePristo, S. D. Augustin, R. Ramaswamy, and H. Rabitz, *J. Chem. Phys.* **71**, 850 (1979).
- ¹⁰M. L. Koszykowski, L. A. Rahn, R. E. Palmer, and M. E. Coltrin, *J. Phys. Chem.* **91**, 41 (1987); L. A. Rahn, R. E. Palmer, M. L. Koszykowski, and D. A. Greenhalgh, *Chem. Phys. Lett.* **133**, 513 (1987).
- ¹¹T.-S. Ho and H. Rabitz, *J. Chem. Phys.* **89**, 5614 (1988); **90**, 1519 (1989); **91**, 7590 (1989); *J. Phys. Chem.* **97**, 13 447 (1993).
- ¹²R. Boyd, T.-S. Ho, H. Rabitz, D. A. Padmavathi, and M. K. Mishra, *J. Chem. Phys.* **101**, 2023 (1994); R. Boyd, T.-S. Ho, H. Rabitz, *ibid.* **103**, 4052 (1995); **106**, 6548 (1997).
- ¹³T.-S. Ho and H. Rabitz, *J. Chem. Phys.* **94**, 2305 (1991); **96**, 7092 (1992).
- ¹⁴H. Heo, T.-S. Ho, K. K. Lehmann, and H. Rabitz, *J. Chem. Phys.* **97**, 852 (1992); T. S. Ho, H. Rabitz, S. E. Choi, and M. I. Lester, *ibid.* **102**, 2282 (1995).
- ¹⁵D. Romanini and K. K. Lehmann, *J. Chem. Phys.* **105**, 81 (1996).
- ¹⁶See, for example, L. Larrabee Strow and A. S. Pine, *J. Chem. Phys.* **89**, 1427 (1988), and references therein.
- ¹⁷S. Temkin, L. Bonamy, J. Bonamy, and D. Robert, *Phys. Rev. A* **47**, 1543 (1993).
- ¹⁸A. S. Pine, *J. Chem. Phys.* **101**, 3444 (1994).
- ¹⁹See, for example, L. Ozanne, N. Van-Thanh, C. Brodbeck, J. P. Bouanich, J. M. Hartmann, and C. Boulet, *J. Chem. Phys.* **102**, 7306 (1995).